

A new multistable double-scroll 4-D hyperchaotic system with no equilibrium point, its bifurcation analysis, synchronization and circuit design

Sundarapandian VAIDYANATHAN, Shaobo HE and Aceng SAMBAS

In this work, we have developed a new 4-D dynamical system with hyperchaos and hidden attractor. First, by introducing a feedback input control into the 3-D Ma chaos system (2004), we obtain a new 4-D hyperchaos system with no equilibrium point. Thus, we derive a new hyperchaos system with hidden attractor. We carry out an extensive bifurcation analysis of the new hyperchaos model with respect to the three parameters. We also carry out probability density distribution analysis of the new hyperchaotic system. Interestingly, the new nonlinear hyperchaos system exhibits multistability with coexisting attractors. Next, we discuss global hyperchaos self-synchronization for the new hyperchaos system via Integral Sliding Mode Control (ISMC). As an engineering application, we realize the new 4-D hyperchaos system with an electronic circuit via MultiSim. The outputs of the MultiSim hyperchaos circuit show good match with the numerical MATLAB plots of the hyperchaos model. We also analyze the power spectral density (PSD) of the hyperchaos of the state variables using MultiSim.

Key words: hyperchaos, hyperchaotic systems, hidden attractors, multistability, sliding mode control and circuit design

1. Introduction

In the recent years, hyperchaotic systems have received good attention in the literature due to their applications in several fields in science and engineering

Copyright © 2021. The Author(s). This is an open-access article distributed under the terms of the Creative Commons Attribution-NonCommercial-NoDerivatives License (CC BY-NC-ND 4.0 <https://creativecommons.org/licenses/by-nc-nd/4.0/>), which permits use, distribution, and reproduction in any medium, provided that the article is properly cited, the use is non-commercial, and no modifications or adaptations are made

S. Vaidyanathan (corresponding author, e-mail: sundarvtu@gmail.com) is with School of Electrical and Computing, Vel Tech University, 400 Feet Outer Ring Road, Avadi, Chennai-600092, Tamil Nadu, India.

S. He (e-mail: hshaobo_123@163.com) is with School of Physics and Electronics, Central South University, Changsha, 410083, China

A. Sambas (e-mail: acengs@umtas.ac.id) is with Department of Mechanical Engineering, Universitas Muhammadiyah Tasikmalaya, Tasikmalaya 46196, West Java, Indonesia.

This work was supported by the Natural Science Foundation of China (Nos. 61901530, 11747150), the China Postdoctoral Science Foundation (No.2019M652791), the Postdoctoral Innovative Talents Support Program (No. BX20180386).

Received 31.08.2020.

such as convection models [1], mechanical models [2, 3], lattices [4], encryption [5–10], neural networks [11, 12], memristive models [13, 14], neuron models [15], finance models [16], generator models [17], circuit models [18, 19], FPGA models [20, 21], etc.

A 3-D chaotic system with a double-scroll attractor was proposed by Ma, Ren and Chen ([22], 2004). By introducing a feedback control, we develop a new double-scroll 4-D hyperchaotic model in this work. The new hyperchaotic model has only two quadratic nonlinear terms in the dynamics. Interestingly, the new hyperchaotic model has no equilibrium point when we take the parameter values to be positive. Chaotic dynamical systems without equilibrium point or with a stable equilibrium point or with infinitely many equilibrium points are said to exhibit hidden attractors [23]. Thus, the new 4-D double-scroll hyperchaotic model has hidden attractor.

Bifurcation analysis of the new hyperchaotic system with respect to each of the three system parameters is discussed in great detail. We also carry out probability density distribution analysis of the new hyperchaotic system. Multistability is a complex behaviour for a nonlinear system which is the existence of several attractors for the same parameter values but different initial conditions [24, 25]. We show that the new double-scroll hyperchaotic system has multistability property.

Many techniques have been proposed in the control literature for the regulation and synchronization of chaotic systems such as nonlinear control [26–28], adaptive control [29–31], fuzzy logic control [32], sliding mode control [33–35], etc. In this work, we use integral sliding mode control (ISMC) to design self-synchronization between the identical states of the new hyperchaos system with itself. Synchronization of hyperchaotic systems has applications in secure communication [36, 37].

As an application in engineering, we design a MultiSim circuit to verify the hyperchaos of the 4-D double-scroll system. We also carry out power spectral design (PSD) analysis of the state variables of the new 4-D double-scroll hyperchaos system. Circuit design of chaotic and hyperchaotic systems is useful for real-world implementations [38].

2. A new double-scroll 4-D hyperchaos system with hidden attractor

In [22], Ma, Ren and Chen (2004) proposed a 3-D chaotic system with the dynamics

$$\begin{cases} \dot{y}_1 = -a(y_1 + y_2), \\ \dot{y}_2 = -y_2 - ay_1y_3, \\ \dot{y}_3 = b + ay_1y_2. \end{cases} \quad (1)$$

We denote the state of the Ma system (1) as $Y = (y_1, y_2, y_3)$.

It is known that the Ma system (1) exhibits chaos for a large range of positive values of the system parameters a and b .

In this work, we show that the Ma system (1) is chaotic for the parameter values taken as $(a, b) = (4, 20)$.

For the initial state $Y(0) = (0.4, 0.5, 0.2)$ and $(a, b) = (4, 20)$, we calculate the Lyapunov characteristic exponents of the Ma system (1) using time-series expansion for $T = 1E5$ seconds as

$$\psi_1 = 1.2012, \quad \psi_2 = 0, \quad \psi_3 = -6.2012. \quad (2)$$

The Lyapunov characteristic exponents spectrum in (2) establishes the chaotic and dissipative nature of the Ma system (1).

It is noted that the Ma system (2) stays invariant when make the transformation of coordinates $(y_1, y_2, y_3) \mapsto (-y_1, -y_2, y_3)$. This makes it clear that the Ma system (2) has rotational symmetry about the y_2 -axis.

When $(a, b) = (4, 20)$, it is easy to calculate the two equilibrium points of the Ma system (1) as follows:

$$B_1 = \begin{bmatrix} \sqrt{5} \\ -\sqrt{5} \\ 0.25 \end{bmatrix} \quad \text{and} \quad B_2 = \begin{bmatrix} -\sqrt{5} \\ \sqrt{5} \\ 0.25 \end{bmatrix}. \quad (3)$$

It is easy to verify that the Jacobian matrices of the Ma system (1) about the equilibrium points have the same spectral values given by

$$\lambda_1 = -6.8840, \quad \lambda_{2,3} = 0.9420 \pm 9.5959 i. \quad (4)$$

Thus, B_1 and B_2 are both saddle-focus equilibrium points, which are unstable.

The Ma system (1) has self-excited, double-scroll chaotic attractor, which is shown in Fig. 1.

In this work, we build a new 4-D system by introducing a feedback control y_4 into the Ma system (1) so that the resulting system is a hyperchaos system with special properties such as hidden attractor.

Our new 4-D system is given by the following dynamics

$$\begin{cases} \dot{y}_1 = -a(y_1 + y_2) + cy_4, \\ \dot{y}_2 = -y_2 - ay_1y_3, \\ \dot{y}_3 = b + ay_1y_2, \\ \dot{y}_4 = y_2. \end{cases} \quad (5)$$

We represent the state of the 4-D system (5) by $Y = (y_1, y_2, y_3, y_4)$. In the model (5), a, b, c are positive parameters.

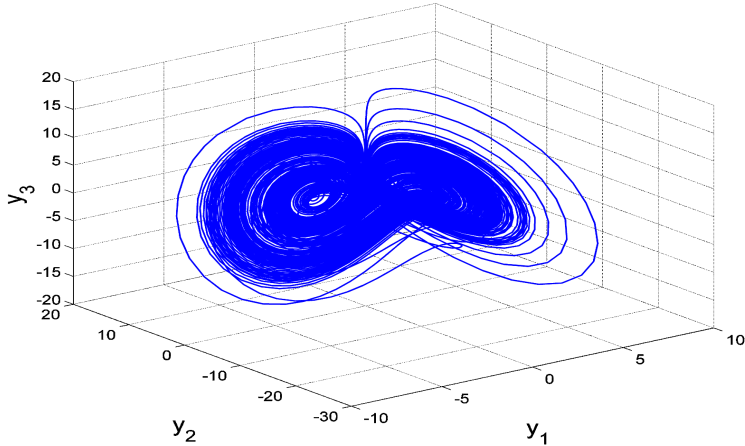


Figure 1: MATLAB simulation showing the double-scroll attractor of the 3-D Ma system (1) for $(a, b) = (4, 20)$ and $Y(0) = (0.4, 0.5, 0.2)$

In this work, we show that the 4-D system (5) is hyperchaotic when we take the parameters as

$$a = 4, \quad b = 20, \quad c = 1. \quad (6)$$

We can verify this fact using MATLAB calculations as follows.

With the initial state $Y(0) = (0.4, 0.5, 0.2, 0.3)$ and $(a, b, c) = (4, 20, 1)$, we can calculate the Lyapunov characteristic exponents of the new 4-D system (5) for $T = 1E5$ seconds as

$$\psi_1 = 1.0375, \quad \psi_2 = 0.2055, \quad \psi_3 = 0, \quad \psi_4 = -6.2433. \quad (7)$$

As the LE spectrum (7) shows, the new 4-D system (5) is a hyperchaotic system with two positive Lyapunov exponents.

Next, we notice that the 4-D system (5) has rotational symmetry about the y_3 coordinate axis as the system (5) stays invariant under the change of coordinates

$$(y_1, y_2, y_3, y_4) \mapsto (-y_1, -y_2, y_3, -y_4). \quad (8)$$

Next, we calculate the equilibrium points of the new system (5). Thus, we proceed to solve the following equations.

$$-a(y_1 + y_2) + cy_4 = 0, \quad (9a)$$

$$-y_2 - ay_1y_3 = 0, \quad (9b)$$

$$b + ay_1y_2 = 0, \quad (9c)$$

$$y_2 = 0. \quad (9d)$$

From (9c) and (9d), we must have $b = 0$, which contradicts the assumption that $b > 0$.

Thus the 4-D system (5) has no equilibrium point when the parameter $b \neq 0$.

Hence, the hyperchaotic system (5) has a *hidden* attractor for the hyperchaotic case (6).

Figures 2–5 show 2-D MATLAB phase plots of the double-scroll 4-D hyperchaotic system (5).

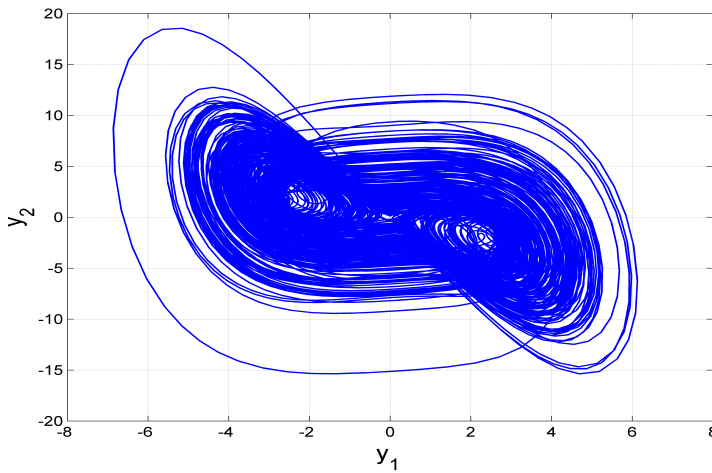


Figure 2: The 2-D MATLAB (y_1, y_2) phase plot of the new double-scroll 4-D hyperchaotic system (5) for $(a, b, c) = (4, 20, 1)$ and $Y(0) = (0.4, 0.5, 0.2, 0.3)$

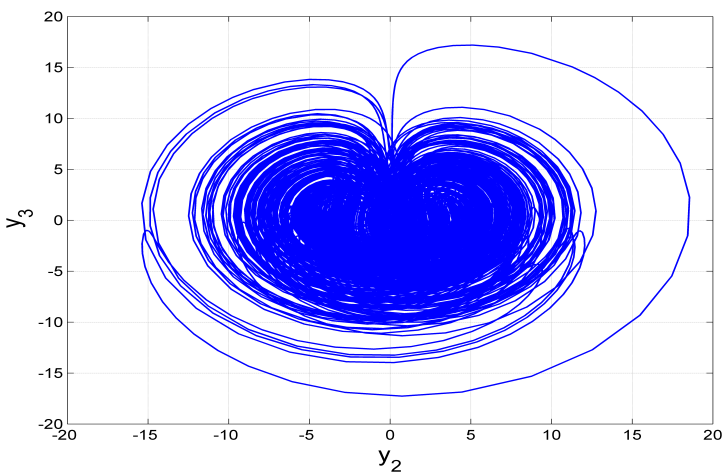


Figure 3: The 2-D MATLAB (y_2, y_3) phase plot of the new double-scroll 4-D hyperchaotic system (5) for $(a, b, c) = (4, 20, 1)$ and $Y(0) = (0.4, 0.5, 0.2, 0.3)$

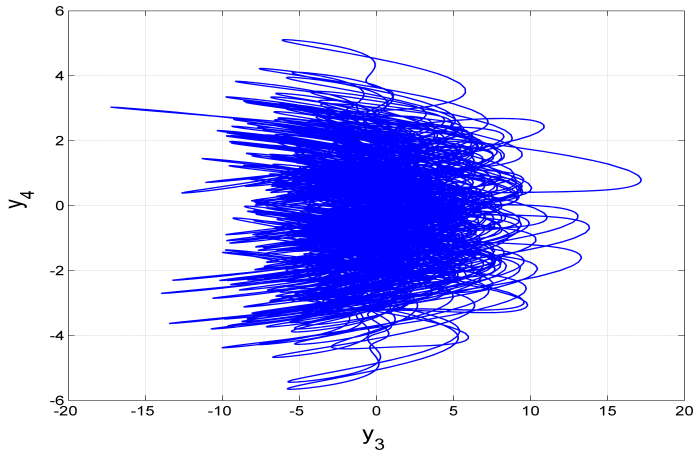


Figure 4: The 2-D MATLAB (y_3, y_4) phase plot of the new double-scroll 4-D hyperchaotic system (5) for $(a, b, c) = (4, 20, 1)$ and $Y(0) = (0.4, 0.5, 0.2, 0.3)$

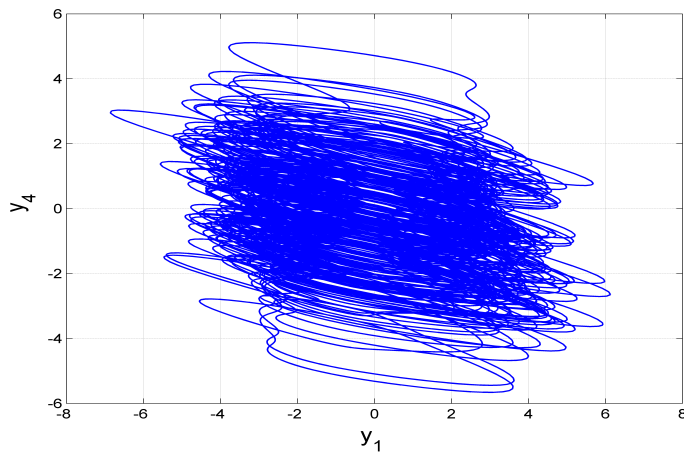


Figure 5: The 2-D MATLAB (y_1, y_4) phase plot of the new double-scroll 4-D hyperchaotic system (5) for $(a, b, c) = (4, 20, 1)$ and $Y(0) = (0.4, 0.5, 0.2, 0.3)$

3. Dynamic analysis of the new double-scroll multistable hyperchaotic system

3.1. Bifurcation analysis of the new system

There are three parameters in the proposed hyperchaotic system, *viz.* a , b and c . Thus, the bifurcation analysis of the system (5) is analyzed based on these three cases. All the three cases are carried out with the initial conditions given by

$$y_1(0) = 2, \quad y_2(0) = 1, \quad y_3(0) = 2, \quad y_4(0) = 4. \quad (10)$$

Case 1. Let $b = 20$, $c = 1$ and a vary from 0 to 10 with the step-size of 0.0024. The bifurcation of the system with the variation of parameter a is shown in Fig. 6a and its corresponding Lyapunov exponents are presented in Fig. 6b. It shows that the system (5) is chaotic and hyperchaotic with the increase of a , but there are many periodic windows. It shows that the largest Lyapunov exponents of the system (5) increase with a , and the system (5) is hyperchaotic in most of the cases.

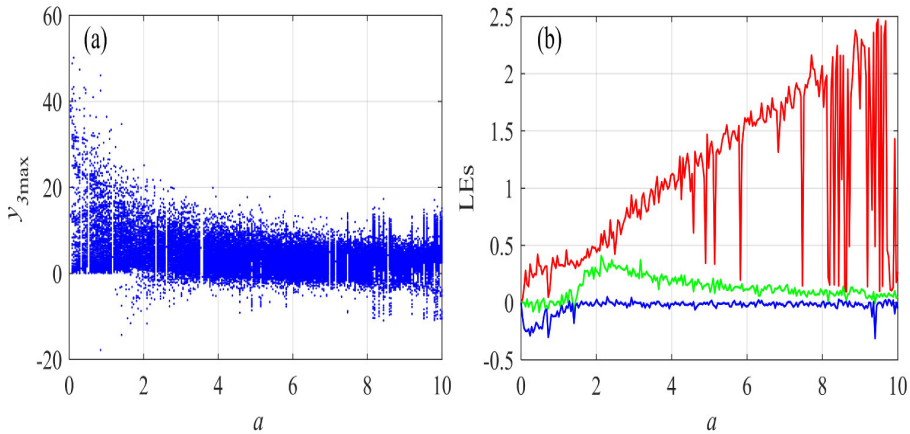


Figure 6: Bifurcation diagram of the hyperchaotic system (5) with the variation of a : (a) Bifurcation diagram and (b) Lyapunov exponents

Case 2. Let $a = 4$, $c = 1$ and b vary from 0 to 50 with the step-size of 0.009. Figure 7 shows the bifurcation diagram and its corresponding Lyapunov

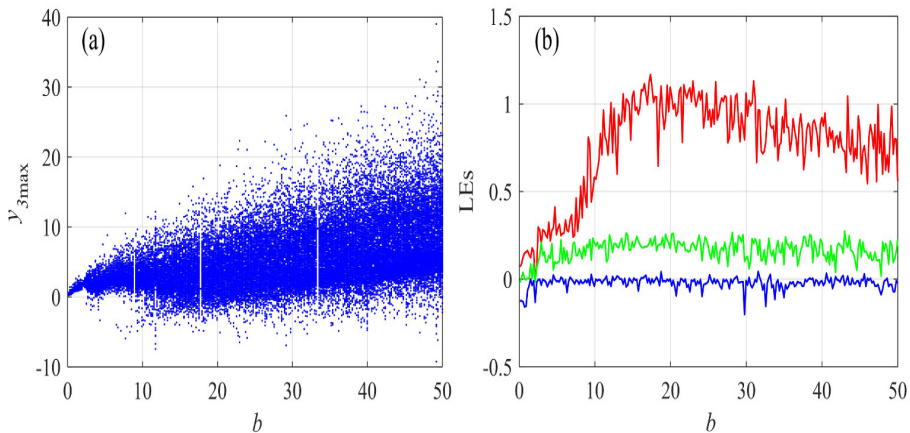


Figure 7: Bifurcation diagram of the hyperchaotic system (5) with the variation of b : (a) Bifurcation diagram and (b) Lyapunov exponents

exponents. As shown in Fig. 7, the system (5) is hyperchaotic with the variation of the parameter b . The largest Lyapunov exponents of the system (5) increases at the beginning stage and then as well. As a result, the system has higher complexity interval of the parameter b in $[15, 25]$, where the system (5) has the largest Lyapunov exponents.

Case 3. Let $a = 4$, $b = 20$ and c vary from 0 to 10 with step-size of 0.009. The bifurcation analysis results in Fig. 8 show that the system has rich dynamics with the increase of the parameter c . When $c > 4$, there are more and more periodic windows and the system (5) becomes into a periodic one. Meanwhile, the largest Lyapunov exponents of the system (5) decrease with the increase of the parameter c , when $c < 4$. Thus for real-world applications of the system (5), the suggested values of the parameter c should be those smaller than 4.

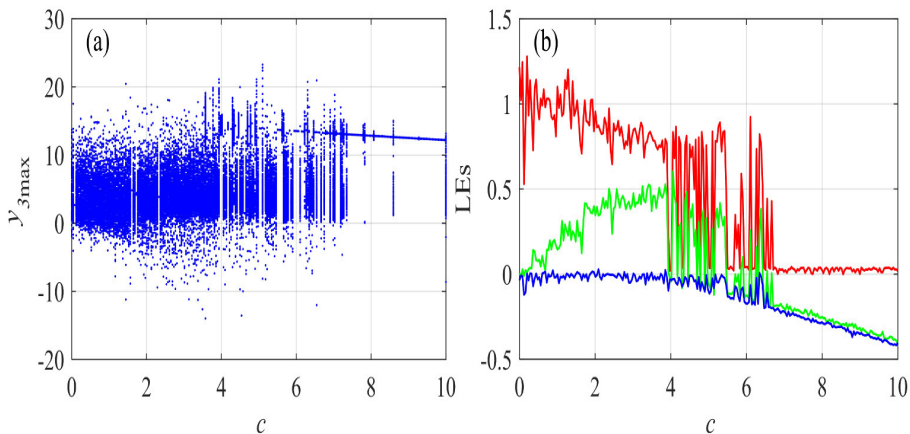


Figure 8: Bifurcation diagram of the hyperchaotic system (5) with the variation of c : (a) Bifurcation diagram and (b) Lyapunov exponents

3.2. Probability density distribution

The probability density distribution analysis of the generated chaotic time series is investigated in this section. The higher and narrower the normal distribution probability density curve is, the smaller the variance is. The smaller the variance means that the data is more concentrated near its mean value. For the nonlinear chaotic time series, it means that the time series is more complex.

We take eight examples to show the probability density distributions of the system (5), where all the cases are carried out with initial condition $(y_1(0), y_2(0), y_3(0), y_4(0)) = (2, 1, 2, 4)$. The first four cases are obtained with $b = 20$, $c = 1$ and $a = 2, 4, 6$ and 8, while the second four cases are obtained with $a = 4$, $c = 1$ and $b = 10, 20, 30$ and 40. As shown in Fig. 9 that the system has

higher and narrower the normal distribution probability density curves when it has larger parameters a and b . Thus, it shows that the system has higher complexity with larger parameters a and b . In fact, the analysis results with probability density curves agree well with the bifurcation analysis results.

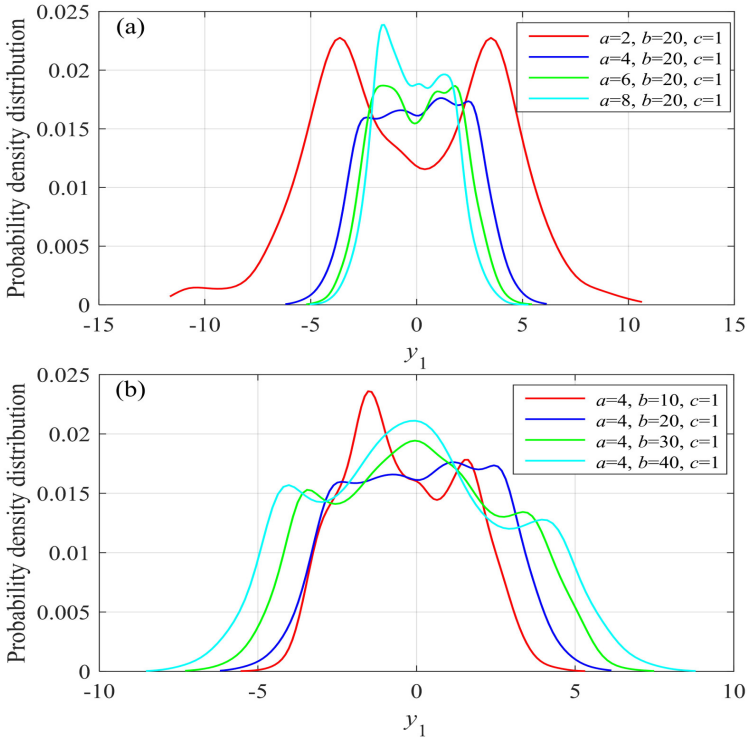


Figure 9: Probability density distribution of the system (5) with different parameters: (a) The parameter a varying; (b) The parameter b varying.

3.3. Multistability and coexisting attractors

Multistability is a special property of a chaotic or a hyperchaotic system which indicates the presence of two or more coexisting attractors for the system for the same set of parameters but different sets of initial conditions.

In this paper, we show that multi-stability exists for the proposed hyperchaotic system (5).

To decide whether the obtained attractor is new or not, we need to consider the size and position of the attractor. We introduce the following method.

For the proposed system (5), we have four state variables, *viz.* y_1, y_2, y_3 and y_4 . Thus, four time-series are obtained, and we also define them as $\{y_i(n) : n = 1, 2, \dots, N \text{ and } i = 1, 2, 3, 4\}$, where N is the length of the time-series.

The position of the attractor is defined by

$$P = [\bar{y}_1, \bar{y}_2, \bar{y}_3, \bar{y}_4]. \quad (11)$$

Here, \bar{y}_i denotes the mean value of the time-series y_i for $i = 1, 2, 3, 4$. The size of each time-series for the attractor is defined as

$$S_i = \max(y_i) - \min(y_i) \quad \text{for } i = 1, 2, 3, 4. \quad (12)$$

Suppose that there are two attractors for the proposed system (5) and their time-series are defined by $\{y_i(n) : n = 1, 2, \dots, N, i = 1, 2, 3, 4\}$ and $\{\tilde{y}_i(n) : n = 1, 2, \dots, N, i = 1, 2, 3, 4\}$.

The error between the positions of the two attractors is given by

$$e_1 = \frac{1}{4} \sqrt{\sum_{i=1}^4 (\bar{y}_i - \tilde{\bar{y}}_i)^2}. \quad (13)$$

The error regarding the sizes of the two attractors is defined by

$$e_2 = \frac{1}{4} \sqrt{\sum_{i=1}^4 (S_i - \tilde{S}_i)^2}. \quad (14)$$

In this paper, we set a parameter *error* to decide whether the obtained attractor is different with the existing ones or not. Namely, if both $e_1 > \text{error}$ and $e_2 > \text{error}$, then the obtained attractor $\{\tilde{y}_i(n) : n = 1, 2, \dots, N, i = 1, 2, 3, 4\}$ is a new attractor. Otherwise, it is not a new attractor. In this paper, the value of *error* is 50.

Let $a = 3, b = 40, c = 3, y_3(0) = 2, y_4(0) = 4$ and the initial conditions $y_1(0)$ and $y_2(0)$ both vary from -10 to 10 with step size of one. The coexisting attractors found in the system (5) are shown in Fig. 10. In fact, there are 34 different kind of the attractors found in the system (5) with the given parameters under different initial conditions. Some of the initial conditions of different attractors are listed in Fig. 10.

In Fig. 10, two different attractors with initial conditions $Y(0) = (-8, 7, 2, 4)$ and $Y(0) = (-10, 6, 2, 4)$ are shown with red color and blue color, respectively.

Let $a = 4, b = 20, c = 1, y_3(0) = 2, y_4(0) = 4$ and the initial conditions $y_1(0)$ and $y_2(0)$ both vary from -10 to 10 with step size of one. The coexisting attractors found in the system (5) are shown in Fig. 11. The attractors may look similar but they have some differences according to the method introduced in this paper. For instance, as shown in Fig. 10, the blue attractor and the red attractor are different since the blue one has holes in the middle of the phase space.

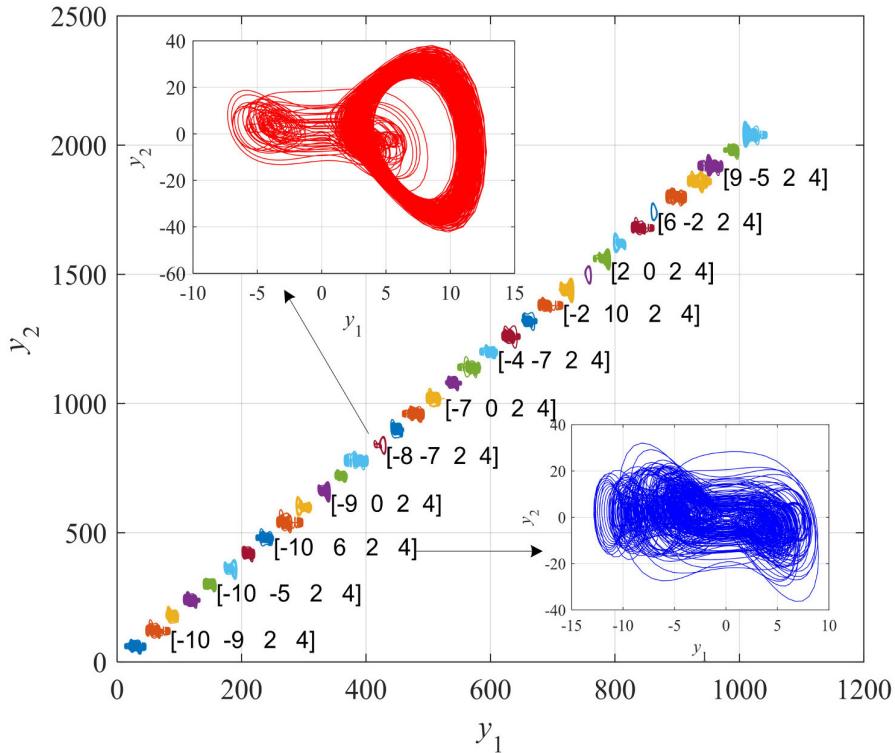


Figure 10: Coexisting attractors of the system (5) with parameters $a = 3$, $b = 40$, $c = 3$

It should be noted that the coexisting attractors as shown in the two figures (Figs. 10 and 11) are overlapped with each other in the phase space $y_1 \in [-15, 15]$ and $y_2 \in [-40, 40]$. The two figures are plotted by considering the distinguishability of different attractors. Meanwhile, the initial conditions are listed in the Figs. 10 and 11. As for the method to detect different coexisting attractors, it is effective for those attractors with different size and positions. Meanwhile, the values of the error should be chosen carefully. A small error could make the algorithm sensitive to the attractors with small difference, but large error could make the method to ignore those attractors with small difference. Due to the limitation of the algorithm which is designed based on the size and position, we cannot guarantee that we found all the coexisting attractors for the system (5).

As a result, the proposed system (5) has multistability with the initial conditions. The system has different number of coexisting attractors with different sets of parameters. It shows that the system has found 34 coexisting attractors with $a = 3$, $b = 40$, $c = 3$ and the given simulation conditions.

If we search the initial space with smaller step-size, more coexisting attractors may be found. Although there are many coexisting attractor for the proposed

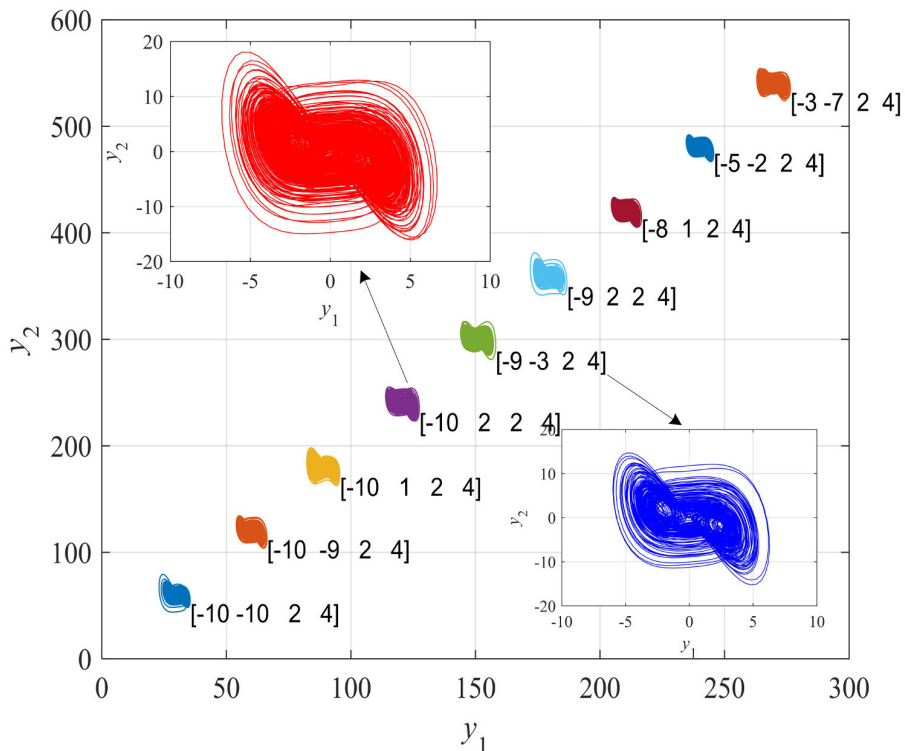


Figure 11: Coexisting attractors of the system (5) with parameters $a = 4$, $b = 20$, $c = 1$

system (5), whether the system (5) has extreme multistability or not needs further investigation.

3.4. Complexity analysis

In this section, multiscale spectral entropy (MSE) algorithm [39, 40] is employed to analyze the complexity of the proposed system (5).

Firstly, complexity of the system (5) with the variation of system parameters a , b and c is analyzed and the results are shown in Fig. 12.

Here, the system parameters and initial conditions are set as the same with those in Figs. 6, 7 and 8.

As shown in Fig. 12, the complexity analysis results of the system (5) matches well with the largest Lyapunov exponents of the system (5). Figure 12 shows that the system (5) has high complexity with proper parameters.

Secondly, complexity of the system in the parameter plane is analyzed. Here, the parameter a varies from 0 to 10 with step size of 0.1, the parameter b varies from 0 to 50 with step size of 0.5 and the parameter c varies from 0 to 4 with step

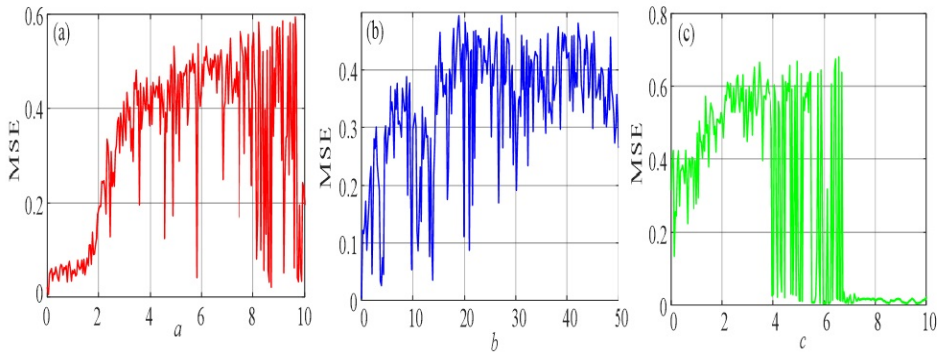


Figure 12: Complexity analysis of the system (5) with (a) a varying, (b) b varying and (c) c varying

size of 0.04. The complexity analysis results in the parameter planes (a, c) and (b, c) are shown in Fig. 13.

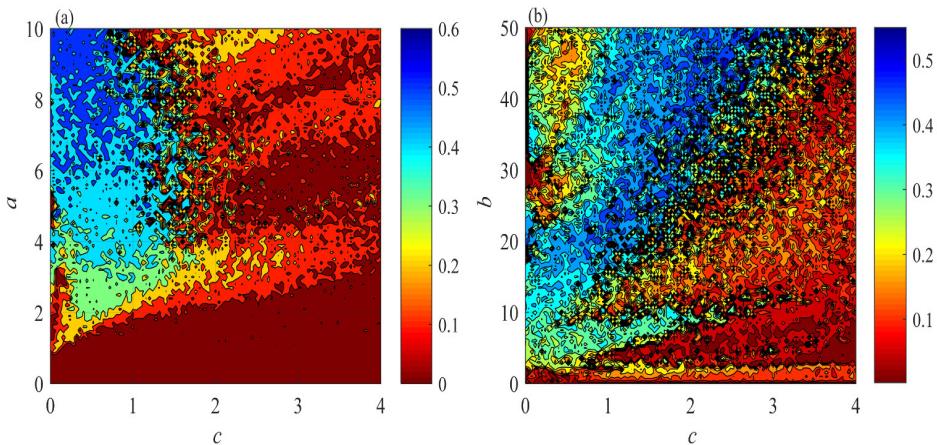


Figure 13: Complexity analysis of the system (5) in the parameter planes: (a) (a, c) -plane and (b) (b, c) -plane

Figure 13 shows that the system (5) has higher complexity in the left side of the parameter planes. In fact, according to the complexity analysis results, the system (5) has higher complexity with smaller parameter c and larger parameters a and b .

Thirdly, the complexity of the system (5) with different initial conditions is analyzed by fixing $z_0 = 2$, $w_0 = 4$ and varying x_0 and y_0 from -10 to 10 . The analysis results are shown in Fig. 14, where Fig. 14a is obtained by fixing $a = 3$, $b = 40$ and $c = 3$ and Fig. 14b is obtained by fixing $a = 4$, $b = 20$ and

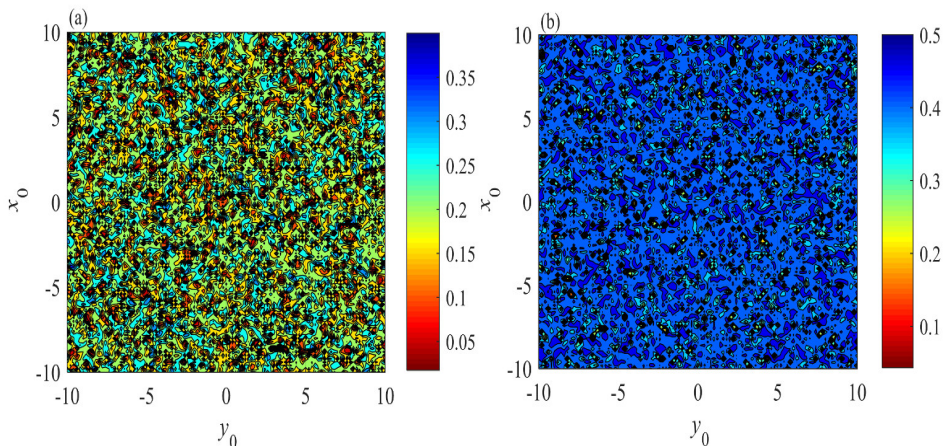


Figure 14: Complexity analysis of the system (5) with different initial conditions by fixing $z_0 = 2, w_0 = 4$ and varying x_0 and y_0 : (a) $a = 3, b = 40, c = 3$ and (b) $a = 4, b = 20, c = 1$

When the system (5) has high complexity, it means that the system is chaotic. When the system (5) has low complexity, it means that the system is non-chaotic including the periodic states. Figure 14 shows that the system (5) has different complexity measure results with different conditions. Compared with case (b), case (a) has more complex behaviors in the initial condition plane. In fact, there are more coexisting attractors in case (a) as shown in Fig. 10. Thus the multistability in the proposed system (5) is verified by the complexity measure algorithm.

4. Self-synchronization of the new double-scroll multistable hyperchaotic system

In this section, we deploy integral sliding mode control (ISMC) to achieve global self-synchronization of the new double-scroll multistable hyperchaotic system with itself (drive-slave systems).

The drive system of the self-synchronization design consists of the new double-scroll multistable hyperchaotic system given by

$$\begin{cases} \dot{y}_1 = -a(y_1 + y_2) + cy_4, \\ \dot{y}_2 = -y_2 - ay_1y_3, \\ \dot{y}_3 = b + ay_1y_2, \\ \dot{y}_4 = y_2. \end{cases} \quad (15)$$

In the drive system (15), $Y = (y_1, y_2, y_3, y_4)$ is the state.

The slave system of the self-synchronization design consists of the new double-scroll multistable hyperchaotic system with controls given by

$$\begin{cases} \dot{z}_1 = -a(z_1 + z_2) + cz_4 + U_1, \\ \dot{z}_2 = -z_2 - az_1z_3 + U_2, \\ \dot{z}_3 = b + az_1z_2 + U_3, \\ \dot{z}_4 = z_2 + U_4. \end{cases} \quad (16)$$

In the slave system (16), $Z = (z_1, z_2, z_3, z_4)$ is the state.

Here, (a, b, c) are constant parameters and U_1, U_2, U_3, U_4 are controls to be designed so as to synchronize the like states of the drive system (15) and slave system (16).

In the usual manner, the self-synchronization error for the new hyperchaotic systems (15) and (16) is defined as follows:

$$\begin{cases} \epsilon_1 = z_1 - y_1, \\ \epsilon_2 = z_2 - y_2, \\ \epsilon_3 = z_3 - y_3, \\ \epsilon_4 = z_4 - y_4. \end{cases} \quad (17)$$

Proceeding next, we calculate the error dynamics for the self-synchronization error as follows:

$$\begin{cases} \dot{\epsilon}_1 = -a(\epsilon_1 + \epsilon_2) + c\epsilon_4 + U_1, \\ \dot{\epsilon}_2 = -\epsilon_2 - a(z_1z_3 - y_1y_3) + U_2, \\ \dot{\epsilon}_3 = a(z_1z_2 - y_1y_2) + U_3, \\ \dot{\epsilon}_4 = \epsilon_2 + U_4. \end{cases} \quad (18)$$

In the control design, we associate an integral sliding surface with each error variable as follows:

$$\begin{cases} S_1 = \epsilon_1 + \mu_1 \int_0^t \epsilon_1(\nu) d\nu, \\ S_2 = \epsilon_2 + \mu_2 \int_0^t \epsilon_2(\nu) d\nu, \\ S_3 = \epsilon_3 + \mu_3 \int_0^t \epsilon_3(\nu) d\nu, \\ S_4 = \epsilon_4 + \mu_4 \int_0^t \epsilon_4(\nu) d\nu. \end{cases} \quad (19)$$

Differentiating the sliding surface equations in (19), the following results are obtained:

$$\begin{cases} \dot{S}_1 = \dot{\epsilon}_1 + \mu_1 \epsilon_1, \\ \dot{S}_2 = \dot{\epsilon}_2 + \mu_2 \epsilon_2, \\ \dot{S}_3 = \dot{\epsilon}_3 + \mu_3 \epsilon_3, \\ \dot{S}_4 = \dot{\epsilon}_4 + \mu_4 \epsilon_4. \end{cases} \quad (20)$$

Thus, we derive the integral sliding manifold controls as follows:

$$\begin{cases} U_1 = a(\epsilon_1 + \epsilon_2) - c\epsilon_4 - \mu_1 \epsilon_1 - \alpha_1 \operatorname{sgn}(S_1) - \beta_1 S_1, \\ U_2 = \epsilon_2 + a(z_1 z_3 - y_1 y_3) - \mu_2 \epsilon_2 - \alpha_2 \operatorname{sgn}(S_2) - \beta_2 S_2, \\ U_3 = -a(z_1 z_2 - y_1 y_2) - \mu_3 \epsilon_3 - \alpha_3 \operatorname{sgn}(S_3) - \beta_3 S_3, \\ U_4 = d(e_x + e_y) - \lambda_w e_w - \tau_w \operatorname{sgn}(\sigma_w) - k_y \sigma_w. \end{cases} \quad (21)$$

By implementing the sliding control law (21), we derive the following closed-loop system:

$$\begin{cases} \dot{\epsilon}_1 = -\mu_1 \epsilon_1 - \alpha_1 \operatorname{sgn}(S_1) - \beta_1 S_1, \\ \dot{\epsilon}_2 = -\mu_2 \epsilon_2 - \alpha_2 \operatorname{sgn}(S_2) - \beta_2 S_2, \\ \dot{\epsilon}_3 = -\mu_3 \epsilon_3 - \alpha_3 \operatorname{sgn}(S_3) - \beta_3 S_3, \\ \dot{\epsilon}_4 = -\mu_4 \epsilon_4 - \alpha_4 \operatorname{sgn}(S_4) - \beta_4 S_4. \end{cases} \quad (22)$$

The main control result of this section on self-synchronization of the new multistable double-scroll hyperchaotic systems is established in the following theorem.

Theorem 1 *The new 4-D multistable double-scroll hyperchaotic models (15) and (16) are synchronized globally by the ISMC law (21) where we assume that $\mu_i, \alpha_i, \beta_i, (i = 1, 2, 3, 4)$ are all positive constants.*

Proof. We start the proof by taking the Lyapunov function defined by

$$V(S_1, S_2, S_3, S_4) = \frac{1}{2} (S_1^2 + S_2^2 + S_3^2 + S_4^2) \quad (23)$$

We note that V takes all non-negative values. Also, $V = 0$ if and only if $S_1 = S_2 = S_3 = S_4 = 0$.

This shows that V is a quadratic and strictly positive definite function on \mathbf{R}^4 . Next, we find that

$$\dot{V} = S_1\dot{S}_1 + S_2\dot{S}_2 + S_3\dot{S}_3 + S_4\dot{S}_4. \quad (24)$$

Using (20) and (22), we can simplify (24) as

$$\dot{V} = \sum_{i=1}^4 S_i(-\alpha_i \operatorname{sgn}(S_i) - \beta_i S_i). \quad (25)$$

Simplifying, we get

$$\dot{V} = - \sum_{i=1}^4 [\alpha_i |S_i| + \beta_i S_i^2] \quad (26)$$

Since $\alpha_i > 0$ and $\beta_i > 0$ for $i = 1, 2, 3, 4$, we conclude that \dot{V} is a negative definite function defined on \mathbf{R}^4 .

Thus, by Lyapunov stability theory, it follows that $S_i(t) \rightarrow 0$, ($i = 1, 2, 3, 4$) as $t \rightarrow \infty$.

Hence, we conclude that $\epsilon_i(t) \rightarrow 0$, ($i = 1, 2, 3, 4$) as $t \rightarrow \infty$.

This completes the proof. □

Next, we carry out MATLAB simulations to illustrate the ISMC design for the self-synchronization of the new multistable double-scroll hyperchaotic models (15) and (16).

The parameters are taken as in the hyperchaos case, *viz.* $(a, b, c) = (4, 20, 1)$.

Let us take the sliding constants for MATLAB simulations as $\alpha_i = 0.2$, $\beta_i = 10$ and $\mu_i = 12$ for $i = 1, 2, 3, 4$.

Let us consider the initial state of the drive system (15) as

$$y_1 = 3.2, \quad y_2 = 10.4, \quad y_3 = 14.8, \quad y_4 = 2.9. \quad (27)$$

Let us take the initial state of the slave system (16) as

$$z_1 = 8.5, \quad z_2 = 2.1, \quad z_3 = 9.7, \quad z_4 = 11.6. \quad (28)$$

The sliding controller design based complete self-synchronization between the new multistable double-scroll hyperchaos models (15) and (16) is illustrated in Figs. 15–19.

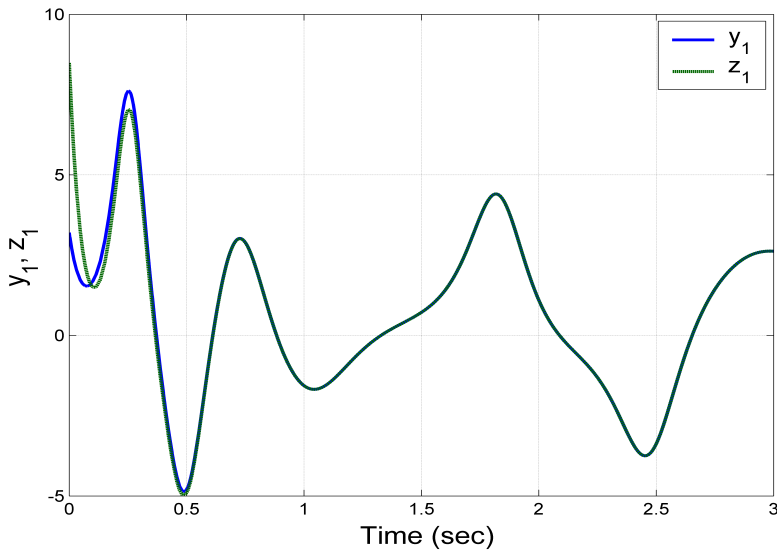


Figure 15: MATLAB plot showing synchronization between y_1 and z_1 for the multistable hyperchaotic systems (15) and (16)

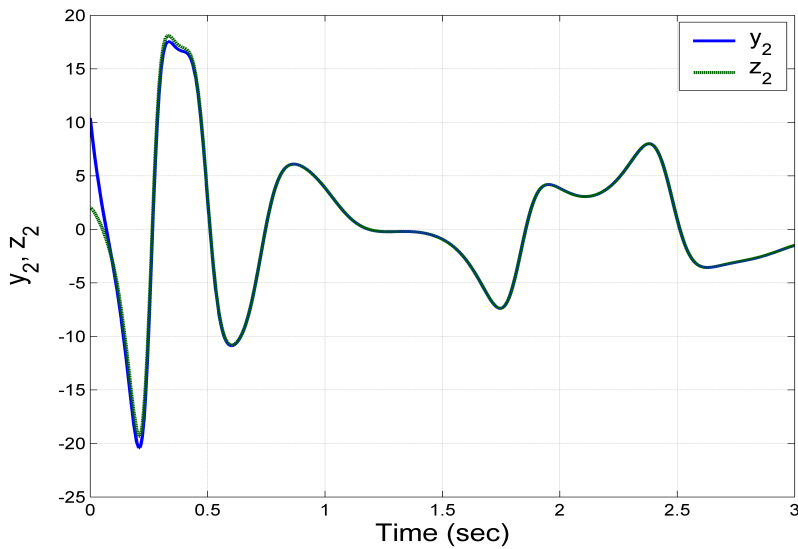


Figure 16: MATLAB plot showing synchronization between y_2 and z_2 for the multistable hyperchaotic systems (15) and (16)

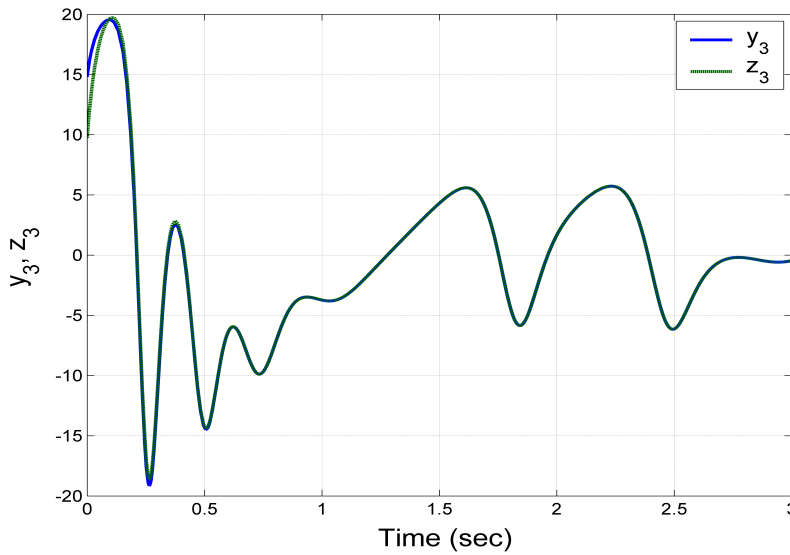


Figure 17: MATLAB plot showing synchronization between y_3 and z_3 for the multistable hyperchaotic systems (15) and (16)

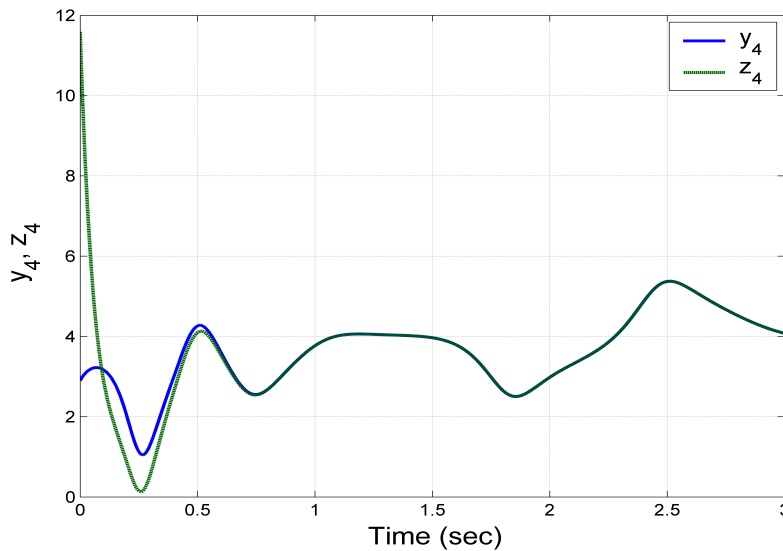


Figure 18: MATLAB plot showing synchronization between y_4 and z_4 for the multistable hyperchaos systems (15) and (16)

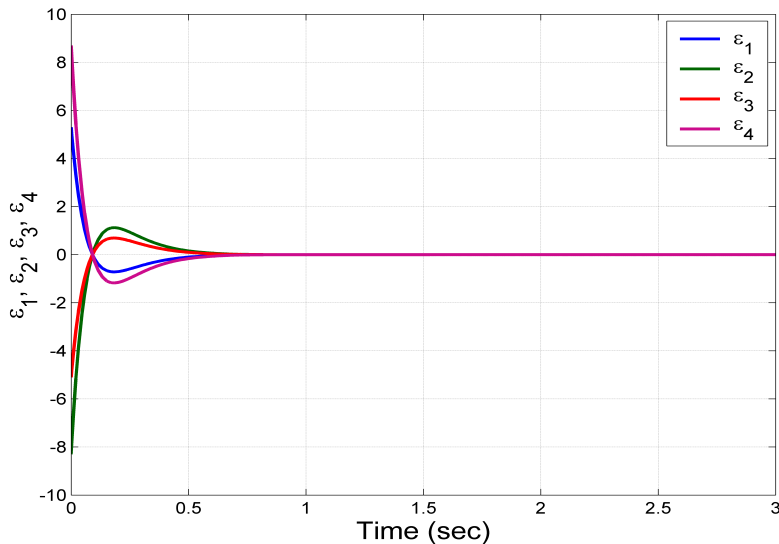


Figure 19: MATLAB plot showing synchronization errors with time-history for the multistable hyperchaotic systems (15) and (16)

5. Circuit simulation of the new 4-D Hyperchaotic system with Hidden Attractors

In this work, we design an electronic circuit using MultiSim to implement the proposed multistable double-scroll hyperchaotic system (5), and verify our findings based on MultiSim simulations.

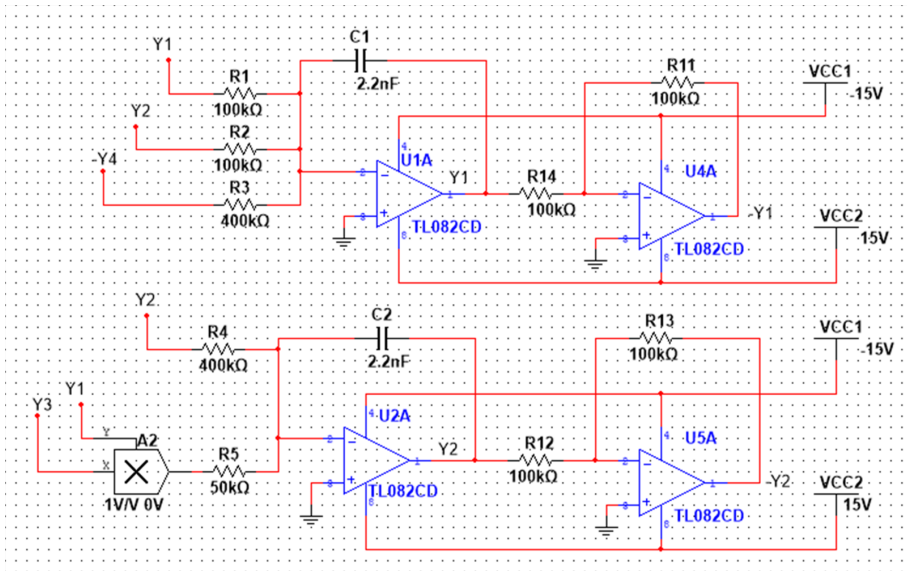
For this purpose, we consider the new hyperchaotic system with hidden attractor whose circuit design is shown in Fig. 20.

For implementation, the four state variables y_1, y_2, y_3, y_4 of the hyperchaotic system (5) are rescaled as follows:

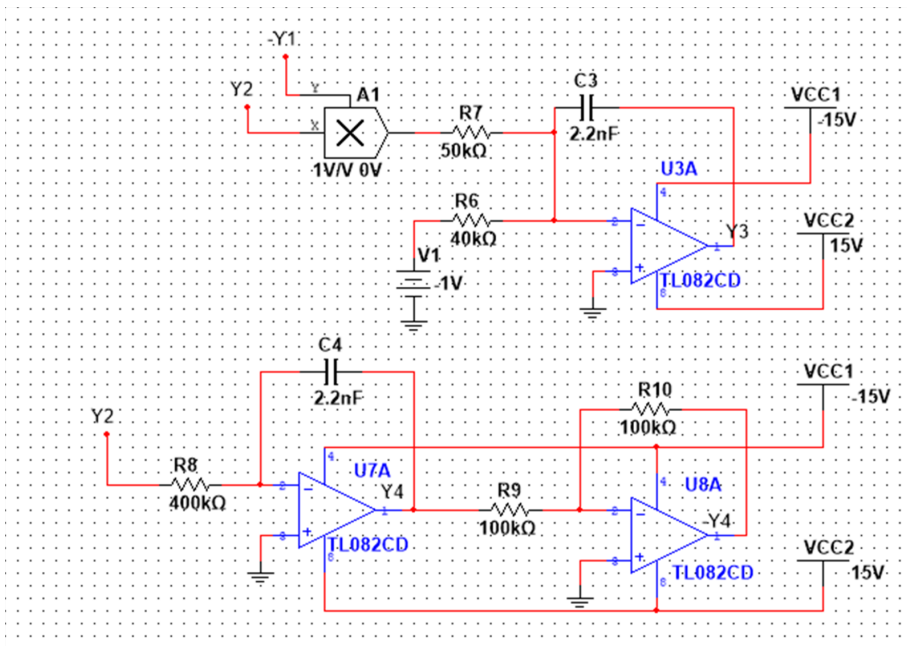
$$Y_1 = \frac{1}{2}y_1, \quad Y_2 = \frac{1}{2}y_2, \quad Y_3 = \frac{1}{2}y_3, \quad Y_4 = \frac{1}{2}y_4. \quad (29)$$

As a result, we transform the hyperchaotic system (5) into the following rescaled system:

$$\begin{cases} \dot{Y}_1 = -a(Y_1 + Y_2) + cY_4, \\ \dot{Y}_2 = -Y_2 - 2aY_1Y_3, \\ \dot{Y}_3 = \frac{b}{2} + 2aY_1Y_2, \\ \dot{Y}_4 = Y_2. \end{cases} \quad (30)$$



(a)



(b)

Figure 20: Circuit design of the hyperchaotic system (30) (a) Y_1 signal and Y_2 signal, (b) Y_3 signal and Y_4 signal

Applying the Kirchhoff laws, the circuit presented in Fig. 20 is described by the following equations:

$$\begin{cases} \dot{Y}_1 = -\frac{1}{C_1 R_1} Y_1 - \frac{1}{C_1 R_2} Y_2 + \frac{1}{C_1 R_3} Y_4, \\ \dot{Y}_2 = -\frac{1}{C_2 R_4} Y_2 - \frac{1}{C_2 R_5} Y_1 Y_3, \\ \dot{Y}_3 = \frac{1}{C_3 R_6} V_1 + \frac{1}{C_3 R_7} Y_1 Y_2, \\ \dot{Y}_4 = \frac{1}{C_4 R_8} Y_2. \end{cases} \quad (31)$$

In (31), Y_1, Y_2, Y_3 and Y_4 correspond to the voltages on the integrators U1A, U2A, U3A and U7A, respectively. The values of components in the circuit are selected as: $R_3 = R_4 = R_8 = 400 \text{ k}\Omega$, $R_5 = R_7 = 50 \text{ k}\Omega$, $R_6 = 40 \text{ k}\Omega$, $R_1 = R_2 = R_9 = R_{10} = R_{11} = R_{12} = R_{13} = R_{14} = 100 \text{ k}\Omega$, $C_1 = C_2 = C_3 = C_4 = 1 \text{ nF}$.

Figures 21–24 depict the MultiSIM outputs of the hyperchaotic circuit (30). Comparing these figures with the MATLAB simulations of the hyperchaotic system (5) depicted in Figs. 2–5, a good qualitative agreement is observed.

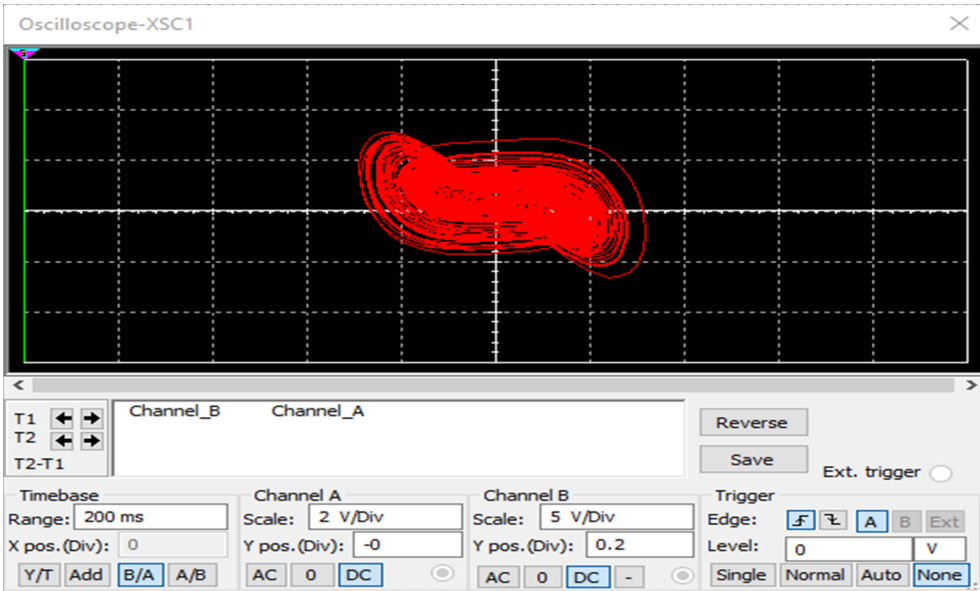


Figure 21: MultiSim circuit simulation showing the multistable double-scroll hyperchaotic attractor of (30) in (Y_1, Y_2) -plane

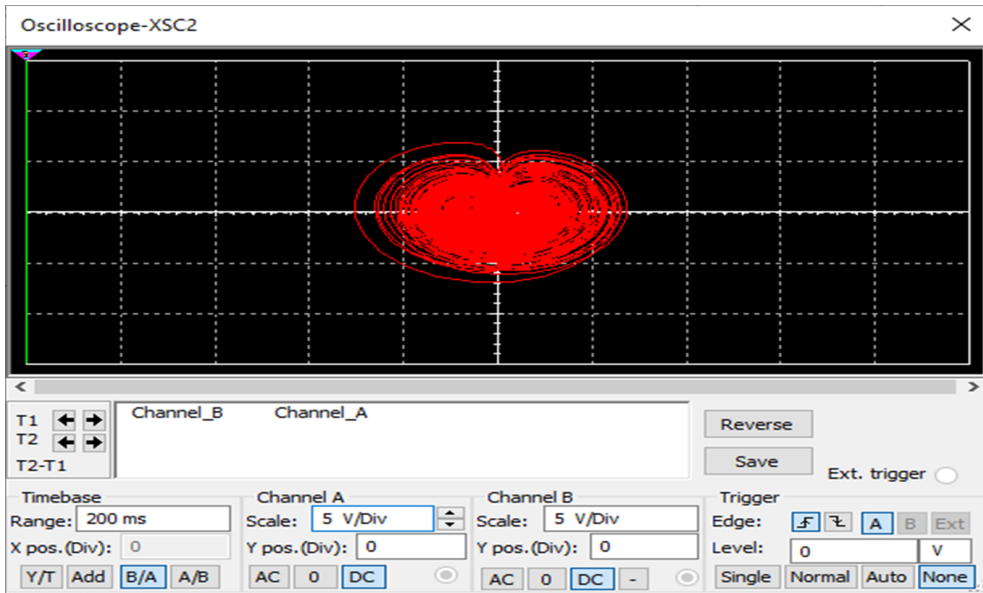


Figure 22: MultiSim circuit simulation showing the multistable double-scroll hyperchaotic attractor of (30) in (Y_2, Y_3) -plane

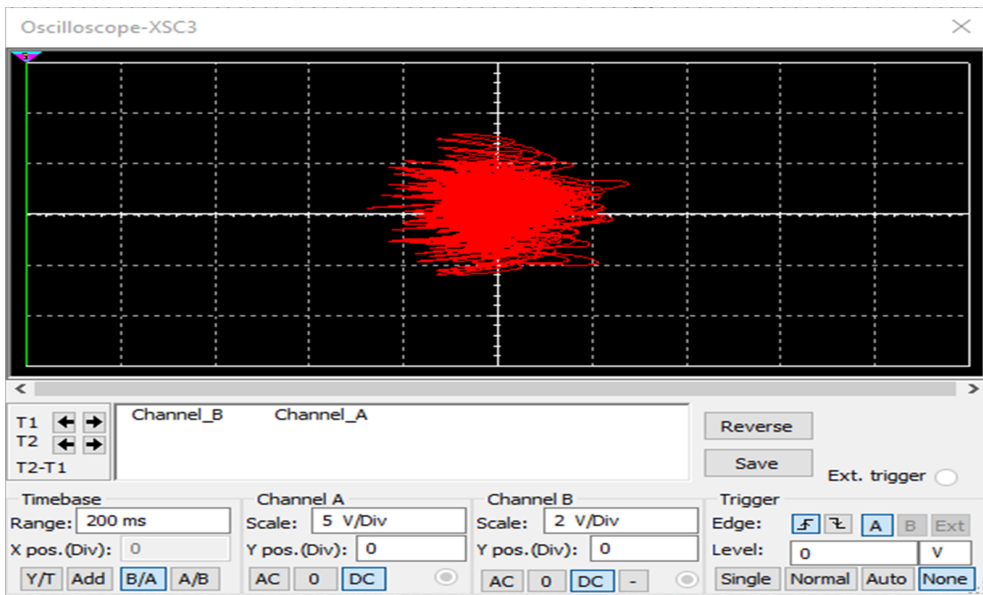


Figure 23: MultiSim circuit simulation showing the multistable double-scroll hyperchaotic attractor of (30) in (Y_3, Y_4) -plane

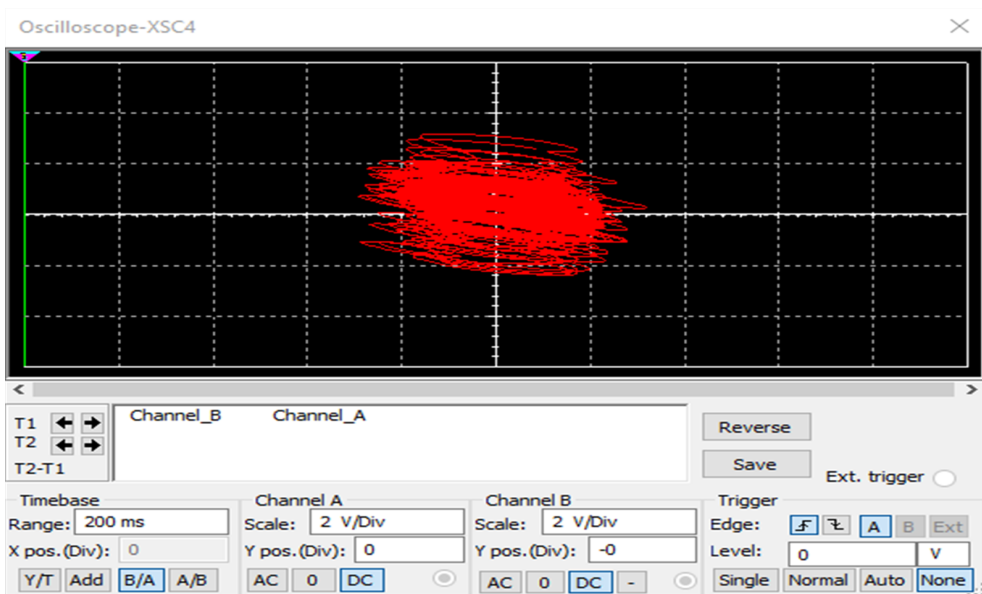


Figure 24: MultiSim circuit simulation showing the multistable double-scroll hyperchaotic attractor of (30) in (Y_1, Y_4) -plane

Figures 25–28 show the Fourier spectral analysis for the four state variables Y_1, Y_2, Y_3 and Y_4 of the hyperchaotic circuit (30). The frequency range is 5 kHz,

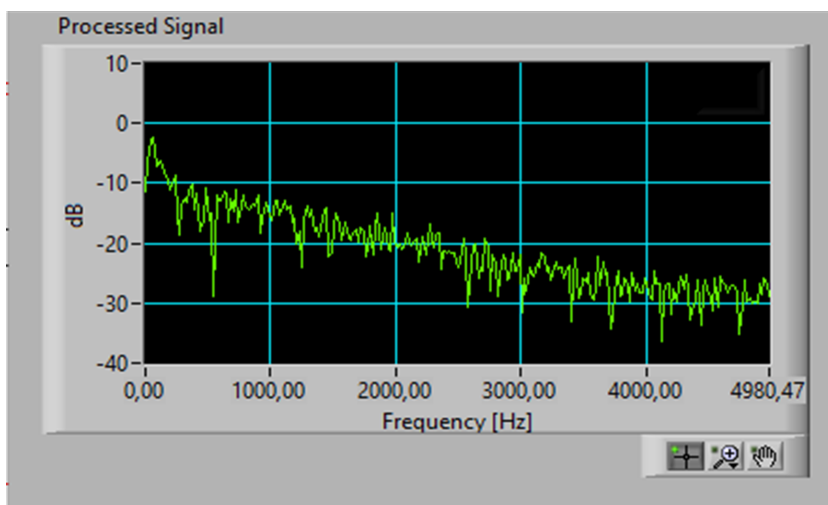


Figure 25: The spectral distribution of the Y_1 signal of the multistable double-scroll hyperchaotic attractor of (30)

and the maximum peak is 1.8 kHz. It corresponds to a prevailing frequency of the implementing oscillating loop. The power spectra of the produced signals are broadband, which are very typical of hyperchaotic signals.

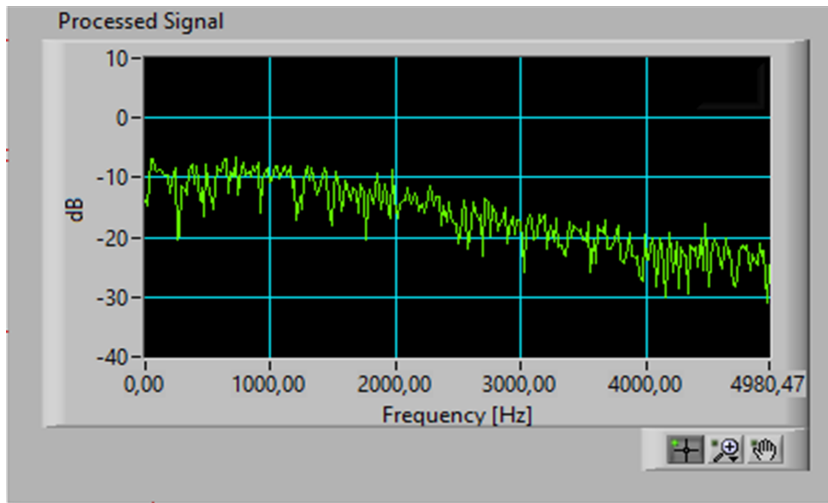


Figure 26: The spectral distribution of the Y_2 signal of the multistable double-scroll hyperchaotic attractor of (30)

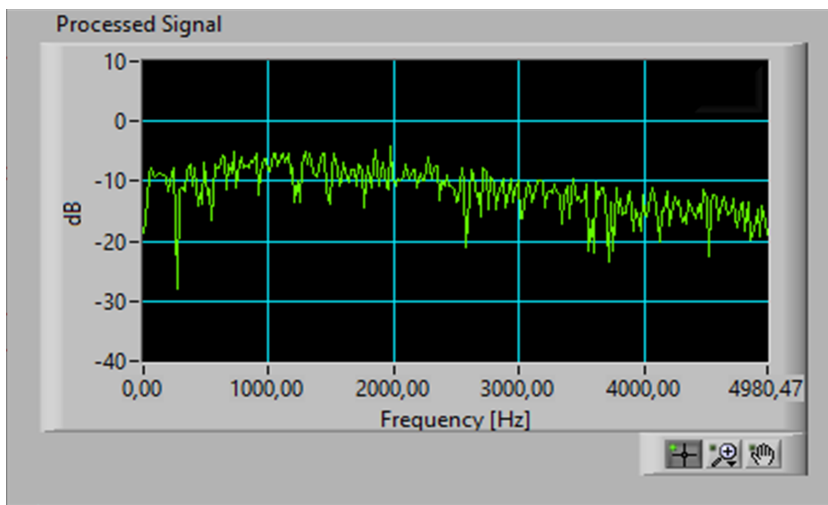


Figure 27: The spectral distribution of the Y_3 signal of the multistable double-scroll hyperchaotic attractor of (30)

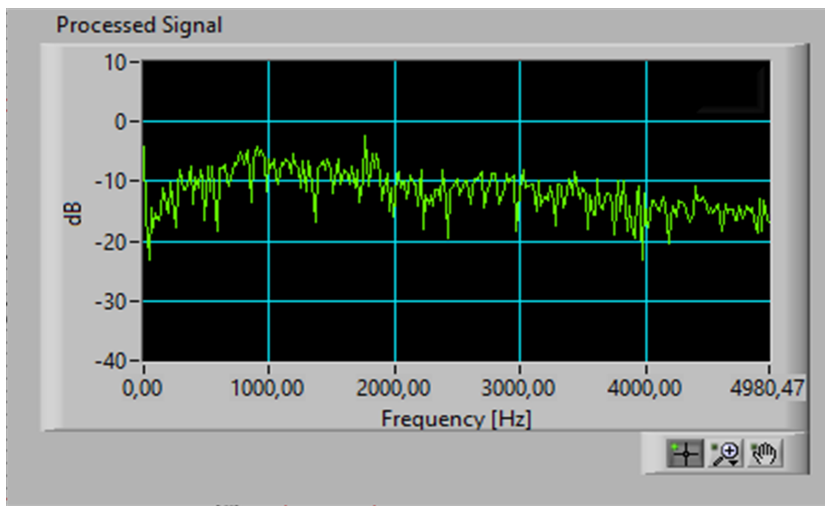


Figure 28: The spectral distribution of the Y_4 signal of the multistable double-scroll hyperchaotic attractor of (30)

6. Conclusions

A new 4-D multistable double-scroll hyperchaotic system with no balance point was reported in this research work. A rigorous bifurcation study of the new hyperchaotic model was presented for the dynamic analysis of the new system with respect to the three parameters. A probability density distribution analysis of the new hyperchaotic model was also presented. We demonstrated that the new nonlinear hyperchaotic system has multistability with coexisting attractors. As control application, global hyperchaos self-synchronization for the new hyperchaotic systems via sliding controller was presented. As an engineering application, we designed a MultiSim electronic circuit for the new 4-D hyperchaotic system. We also analyzed the power spectral density (PSD) of the state variables of the hyperchaotic system using MultiSim.

References

- [1] F.F. FRANCO, E. REMPEL, and P.R. MUNOZ: Crisis and hyperchaos in a simplified model of magnetoconvection, *Physica D: Nonlinear Phenomena*, **406** (2020), Article ID 132417.
- [2] M. STENDER, M. JAHN, N. HOFFMAN, and J. WALLASCHEK: Hyperchaos coexisting with periodic orbits in a frictional oscillator, *Journal of Sound and Vibration*, **472** (2020), Article ID 115203.

-
- [3] A.Y. SHVETS and V.A. SIRENKO: Scenarios of transitions to hyperchaos in nonideal oscillating systems, *Journal of Mathematical Sciences*, **243**(2) (2019), 338–346.
- [4] J. SINGHA and N. GUPTA: Chimera states in globally coupled sine circle map lattices: Spatiotemporal intermittency and hyperchaos, *Physics Letters, Section A: General, Atomic and Solid State Physics*, **384**(11) (2020), Article ID 126225.
- [5] C. XU, J. SUN, and C. WANG: An image encryption algorithm based on random walk and hyperchaotic systems, *International Journal of Bifurcation and Chaos*, **30**(4) (2020), Article ID 20500601.
- [6] P.T. AKKASALIGAR and S. BIRADAR: Selective medical image encryption using DNA cryptography, *Information Security Journal*, **29**(2) (2020), 91–101.
- [7] S. CHENG, L. WANG, N. AO, and Q. HAN: A selective video encryption scheme based on coding characteristics, *Symmetry*, **12**(3) (2020), Article ID 332.
- [8] Y. WAN, S. GU, and B. DU: A new image encryption algorithm based on composite chaos and hyperchaos combined with DNA coding, *Entropy*, **22**(2) (2020), Article ID 171.
- [9] C. ZHONG and M.S. PAN: Encryption algorithm based on scrambling substitution of new hyperchaotic Chen system, *Chinese Journal of Liquid Crystals and Displays*, **35**(1) (2020), 91–97.
- [10] J.X. CUI, G.D. LI, L.L. WANG, and C. MA: Colour image encryption algorithm based on hyperchaos and DNA sequences, *International Journal of Information and Communication Technology*, **16**(3) (2020), 230–244.
- [11] H. LIN and C. WANG: Influences of electromagnetic radiation distribution on chaotic dynamics of a neural network, *Applied Mathematics and Computation*, **369** (2020), Article ID 124840.
- [12] H. LIN, C. WANG, and Y. TAN: Hidden extreme multistability with hyperchaos and transient chaos in a Hopfield neural network affected by electromagnetic radiation, *Nonlinear Dynamics*, **99**(3) (2020), 2369–2386.
- [13] F. LI, C. TAI, H. BAO, J. LUO, and B. BAO: Hyperchaos, quasi-period and co-existing behaviors in second-order-memristor-based jerk circuit, *European Physical Journal: Special Topics*, **229**(6-7) (2020), 1045–1058.

- [14] B.A. MEZATIO, M. MOTCHONGOM TINGUE, R. KENGNE, A. TCHAGNA KOUANOU, T. FOZIN FONZIN, and R. TCHITNGA: Complex dynamics from a novel memristive 6D hyperchaotic autonomous system, *International Journal of Dynamics and Control*, **8**(1) (2020), 70–90.
- [15] S. WANG, S. HE, K. RAJAGOPAL, A. KARTHIKEYAN and K. SUN: Route to hyperchaos and chimera states in a network of modified Hindmarsh-Rose neuron model with electromagnetic flux and external excitation, *European Physical Journal: Special Topics*, **229**(6-7) (2020), 929–942.
- [16] B. XIN, W. PENG, Y. KWON, and Y. LIU: Modeling, discretization, and hyperchaos detection of conformable derivative approach to a financial system with market confidence and ethics risk, *Advances in Difference Equations*, **2019**(1) (2019), Article ID 138.
- [17] N. STANKEVICH, A. KUZNETSOV, E. POPOVA and E. SELEZNEV: Chaos and hyperchaos via secondary Neimark–Sacker bifurcation in a model of radio-physical generator, *Nonlinear Dynamics*, **97**(4) (2019), 2355–2370.
- [18] A. SAMBAS, S. VAIDYANATHAN, S. ZHANG, Y. ZENG, M.A. MOHAMED, and M. MAMAT: A new double-wing chaotic system with coexisting attractors and line equilibrium: Bifurcation analysis and electronic circuit simulation, *IEEE Access*, **7** (2019), 115454–115462.
- [19] C. VOLOS, J.O. MAAITA, S. VAIDYANATHAN, V.T. PHAM, I. STOUBOULOS, and I. KYPRIANIDIS: A novel four-dimensional hyperchaotic four-wing system with a saddle-focus equilibrium, *IEEE Transactions on Circuits and Systems II: Express Briefs*, **64**(3) (2016), 339–343.
- [20] I. KOYUNCU, M. ALCIN, M. TUNA, I. PEHLIVAN, M. VARAN, and S. VAIDYANATHAN: Real-time high-speed 5-D hyperchaotic Lorenz system on FPGA, *International Journal of Computer Applications in Technology*, **61**(3) (2019), 152–165.
- [21] A. SAMBAS, S. VAIDYANATHAN, E. TLELO-CUAUTLE, S. ZHANG, O. GUILLEN-FERNANDEZ, SUKONO, Y. HIDAYAT, and G. GUNDARA: A novel chaotic system with two circles of equilibrium points: Multistability, electronic circuit and FPGA realization, *Electronics*, **8**(11) (2019), Article ID 1211.
- [22] J.H. MA, B. REN, and Y.S. CHEN: Impulsive control of chaotic attractors in nonlinear chaotic systems, *Applied Mathematics and Mechanics*, **25**(9) (2004), 971–976.
- [23] S. VAIDYANATHAN, A.T. AZAR, A. AKGUL, C.H. LIEN, S. KACAR, and U. CAVUSOGLU: A memristor-based system with hidden hyperchaotic attractors, its circuit design, synchronisation via integral sliding mode control

- and an application to voice encryption, *International Journal of Automation and Control*, **13**(6) (2019), 644–647.
- [24] G. Li, Y. Yue, J. Xie, and C. Grebogi: Multistability in a quasiperiodically forced piecewise smooth dynamical system, *Communications in Nonlinear Science and Numerical Simulation*, **84** (2020), Article ID 105165.
- [25] R.W. TAPCHE, Z.T. NJITACKE, J. KENGNE, and F.B. PELAP: Complex dynamics of a novel 3D autonomous system without linear terms having line of equilibria: coexisting bifurcations and circuit design, *Analog Integrated Circuits and Signal Processing*, **103**(1) (2020), 57–71.
- [26] S. VAIDYANATHAN: Output regulation of Arneodo-Couillet chaotic system, *Communications in Computer and Information Science*, **133** (2011), 98–107.
- [27] S. VAIDYANATHAN: Output regulation of the unified chaotic system, *Communications in Computer and Information Science*, **198** (2011), 1–9.
- [28] C.K. VOLOS, V.T. PHAM, S. VAIDYANATHAN, I.M. KYPRIANIDIS, and I.N. STOUBOULOS: Synchronization phenomena in coupled Colpitts circuits, *Journal of Engineering Science and Technology Review*, **8**(2) (2015), 142–151.
- [29] S. VAIDYANATHAN: Chaos in neurons and adaptive control of Birkhoff-Shaw strange chaotic attractor, *International Journal of PharmTech Research*, **8**(5), (2015), 956–963.
- [30] S. VAIDYANATHAN: Global chaos synchronization of the forced Van der Pol chaotic oscillators via adaptive control method, *International Journal of PharmTech Research*, **8**(6) (2015), 156–166.
- [31] S. VAIDYANATHAN: Hybrid chaos synchronization of 3-cells cellular neural network attractors via adaptive control method, *International Journal of PharmTech Research*, **8**(8) (2015), 61–73.
- [32] S. VAIDYANATHAN and A.T. AZAR: Takagi-Sugeno fuzzy logic controller for Liu-Chen four-scroll chaotic system, *International Journal of Intelligent Engineering Informatics*, **4**(2) (2016), 135–150.
- [33] S. VAIDYANATHAN, C. VOLOS, and V.T. PHAM: Global chaos control of a novel nine-term chaotic system via sliding mode control, *Studies in Computational Intelligence*, **576** (2015), 571–590.

- [34] S. VAIDYANATHAN: Analysis and synchronization of the hyperchaotic Yu-jun systems via sliding mode control, *Advances in Intelligent Systems and Computing*, **176** (2012), 329–337.
- [35] S. VAIDYANATHAN and C.H. LIEN: *Applications of Sliding Mode Control in Science and Engineering*, Belin, Springer, 2017.
- [36] S.M. YU and S.S. QIU: Secure communication system via hyperchaos, *Chinese Journal of Radio Science*, **16**(2) (2001), 266.
- [37] D.A. MILLER, B. BAZUIN, D. KERR, and G. GRASSI: Experimental performance of a coherent communication system based on hyperchaos synchronization, *Midwest Symposium on Circuits and Systems*, **3** (2002), 111516–111519.
- [38] X. MIN, X. WANG, P. ZHOU, S. YU, and H.H.C. IU: An optimized memristor-based hyperchaotic system with controlled hidden attractors, *IEEE Access*, **7** (2019), 124641–124646.
- [39] S. HE, K. SUN, and H. WANG: Complexity analysis and DSP implementation of the fractional-order Lorenz hyperchaotic system, *Entropy*, **17**(12) (2015), 8299–8311.
- [40] S. HE and S. BANERJEE: Complex dynamics and multiple coexisting attractors in a fractional-order microscopic chemical system, *European Physical Journal: Special Topics*, **288** (2019) 195–207.